

Dynamical Tides in Eccentric Binaries Containing Massive Main-Sequence Stars: Analytical Expressions

Yubo Su¹, Dong Lai¹

¹ *Cornell Center for Astrophysics and Planetary Science, Department of Astronomy, Cornell University, Ithaca, NY 14853, USA*

Accepted XXX. Received YYY; in original form ZZZ

ABSTRACT

Tidal evolution of eccentric binary systems containing at least one massive main-sequence (MS) star plays an important role in the formation scenarios of merging compact-object binaries. The dominant dissipation mechanism in such systems involves tidal excitation of outgoing internal gravity waves at the convective-radiative boundary and dissipation of the waves at the stellar envelope/surface. We have derived analytical expressions for the tidal torque and tidal energy transfer rate in such binaries for arbitrary orbital eccentricities and stellar rotation rates. These expressions can be used to study the spin and orbital evolution of eccentric binaries containing massive MS stars, such as the progenitors of merging neutron star binaries. Applying our results to the PSR J0045-7319 system, which has a massive B-star companion and an observed, rapidly decaying orbit, we find that for the standard radius of convective core based on non-rotating stellar models, the B-star must have a significant retrograde and differential rotation in order to explain the observed orbital decay rate. Alternatively, we suggest that the convective core may be larger as a result of rapid stellar rotation and/or mass transfer to the B-star in the recent past during the post-MS evolution of the pulsar progenitor.

Key words: stars:binaries stars:rotation

1 INTRODUCTION

The physics of tidal dissipation in massive, main-sequence (MS) stars (i.e. having a convective core and radiative envelope) under the gravitational influence of a companion was first studied by Zahn (1975) (see also Savonije & Papaloizou 1983; Goldreich & Nicholson 1989). The dominant dissipation mechanism is through the *dynamical tide*, in which the time-dependent tidal potential of the companion excites internal gravity waves (IGWs) at the convective-radiative boundary (RCB). As the wave propagates towards the surface, its amplitude grows, and the wave dissipates efficiently (Zahn 1975; Goldreich & Nicholson 1989; Su et al. 2020). The contribution due to viscous dissipation in the convective core is expected to be subdominant.

The original expression describing the torque due to dynamical tides by Zahn (1975) is very sensitive to the global properties of the star. Kushnir et al. (2017) present an updated derivation of the tidal torque that depends only on the local stellar properties near the RCB, eliminating many uncertainties from the Zahn’s original expression. In Zaldarriaga et al. (2018), the authors use the new expression to study tidal synchronization in binaries consisting of a Wolf-Rayet star and a black hole, the likely progenitors to merging black-hole binaries observed by LIGO/VIRGO.

These previous works all apply to nearly circular binaries. However, massive stars can often be found in high-eccentricity (high-e) systems, such as binaries consisting of one MS star and one neutron star (NS). The NS is formed with a large kick velocity (e.g. Lai et al. 2001; Janka et al. 2021), giving rise to a high-e binary. Several such high-e MS-NS systems have been discovered (e.g. Kaspi et al. 1994; Johnston et al. 1994; Champion et al. 2008). These are the progenitors of double NS systems (e.g. Tauris et al. 2017). An important

issue is to understand whether such high-e systems can circularize prior to mass transfer or a common envelope phase (Vigna-Gómez et al. 2020; Vick et al. 2021).

The purpose of this paper is to derive easy-to-use, analytical expressions for the effects of dynamical tides for high-e binaries with massive MS stellar companions. In Section 2, we summarize the equations of dynamical tides involving IGWs in circular binaries and existing techniques for studying high-e systems. In Section 3, we evaluate the effect of dynamical tides in high-e systems containing massive MS stellar companions, including the torque and orbital decay rate. In Section 4, we apply our results to the pulsar-MS binary J0045-7319, for which a non-zero orbital decay rate has been measured. Finally, we summarize our results and discuss the uncertainties in Section 5.

2 DYNAMICAL TIDES IN MASSIVE STARS

2.1 Circular Binaries

We first review the case where the binary is circular. Let M be the mass of the MS star, M_2 the mass of the companion, a the semimajor axis of the binary, and Ω the angular frequency (mean motion) of the binary. The tidal torque exerted on the star by the companion due to tidal excitation of IGWs at the RCB is (Kushnir et al. 2017)

$$T_{\text{circ}}(\omega) = T_0 \operatorname{sgn}(\omega) \left| \frac{\omega}{\Omega} \right|^{8/3}, \quad (1)$$

where

$$T_0 \equiv \beta_2 \frac{GM_2^2 r_c^5}{a^6} \left(\frac{\Omega}{\sqrt{GM_c/r_c^3}} \right)^{8/3} \frac{\rho_c}{\bar{\rho}_c} \left(1 - \frac{\rho_c}{\bar{\rho}_c} \right)^2, \quad (2)$$

$$\beta_2 \equiv \left[\frac{r_c}{g_c} \left(\frac{dN^2}{d \ln r} \right)_{r=r_c} \right]^{-1/3} \left[\frac{3^2 \Gamma^2 (1/3)}{40\pi 12^{2/3}} \alpha^2 \right]. \quad (3)$$

Here, $\omega \equiv 2\Omega - 2\Omega_s$ is the tidal forcing frequency, Ω_s is the spin of the MS star, N is the Brünt-Vaisala frequency, r is the radial coordinate within the star, and r_c , M_c , g_c , ρ_c , and $\bar{\rho}_c$ are the radius of the RCB, the mass contained within the convective core, the gravitational acceleration at the RCB, the stellar density at the RCB, and the average density of the convective core respectively. Γ is the gamma function, α is a numerical constant of order unity given by Eq. (A32) of [Kushnir et al. \(2017\)](#), and $\beta_2 \approx 1$ for a large range of stellar models (Fig. 2 of [Kushnir et al. 2017](#)). In Eq. (1), we have expressed the various factors such that T_0 contains all the spin-independent terms.

The above result (Eq. 1) assumes that tidally excited IGWs dissipate completely as they propagate outwards towards the stellar surface. Such dissipation can happen either through radiative damping or nonlinear effects. Recent hydrodynamical simulations of the IGW breaking process in the stellar envelope ([Su et al. 2020](#)) show that the nonlinear damping of the outward-propagating IGWs is due to the development of a narrow critical layer. This critical layer divides the star into a asynchronously-rotating interior and a synchronously-rotating exterior (see [Goldreich & Nicholson 1989](#)), and it efficiently absorbs the angular momentum of the incident IGWs ($\sim 70\%$ of incident flux, [Su et al. 2020](#)). If the IGWs instead reflect before dissipating completely, then standing waves are set up in the stellar interior. These internal oscillations then dissipate due to radiative damping and nonlinear mode couplings (for the former, see e.g. [Lai 1996; Lai 1997; Kumar & Quataert 1997, 1998](#), and for the latter, see e.g. [O’Leary & Burkart 2014](#)). Except when a tidal forcing frequency is resonant with a stellar oscillation mode, the traveling-wave assumption represents an upper bound on the tidal torque (see e.g. [Yu et al. 2020, 2021](#) concerning tidal dissipation in white dwarf binaries).

Note additionally that we use Eq. (1) from [Kushnir et al. \(2017\)](#) instead of the classic expression from [Zahn \(1975\)](#), which is given by:

$$T_{\text{circ}}^{(\text{Zahn})}(\omega) = \frac{3}{2} \frac{GM_2^2 R^5}{a^6} E_2 \left(\frac{\omega}{\sqrt{GM/R^3}} \right)^{8/3}, \quad (4)$$

where M and R are the mass and radius of the MS star and E_2 is a numerical parameter obtained by integrating over the entire star. The fitting formula $E_2 = 1.592 \times 10^{-9} (M/M_\odot)^{2.84}$ as given by [Hurley et al. \(2002\)](#) is commonly used, which varies by many orders of magnitude for different stars. Moreover, $T_{\text{circ}}^{(\text{Zahn})}$ depends on M and R , properties of the entire star, when the tidal torque is entirely generated at the RCB. For these reasons, the expression by [Kushnir et al. \(2017\)](#) is preferred.

2.2 Eccentric Binaries

The gravitational potential of an eccentric companion at the quadrupole order can be decomposed as a sum over circular orbits

(e.g. [Storch & Lai 2013; Vick et al. 2017](#)):

$$U(\mathbf{r}, t) = \sum_{m=-2}^2 U_{2m}(\mathbf{r}, t), \quad (5)$$

$$U_{2m}(\mathbf{r}, t) = -\frac{GM_2 W_{2m} r^2}{D(t)^3} Y_{2m}(\theta, \phi) e^{-imf(t)},$$

$$= -\frac{GM_2 W_{2m} r^2}{a^3} Y_{2m}(\theta, \phi) \sum_{N=-\infty}^{\infty} F_{Nm} e^{-iN\Omega t}. \quad (6)$$

Here, the coordinate system is centered on the MS star, (r, θ, ϕ) are the radial, polar, and azimuthal coordinates of \mathbf{r} respectively, $W_{2\pm 2} = \sqrt{3}\pi/10$, $W_{2\pm 1} = 0$, $W_{20} = -\sqrt{\pi}/5$, $D(t)$ is the instantaneous distance to the companion, f is the true anomaly, and Y_{lm} denote the spherical harmonics. F_{Nm} denote the *Hansen coefficients* for $l = 2$ (also denoted X_{2m}^N in [Murray & Dermott 1999](#)), which are the Fourier coefficients of the perturbing function, i.e.

$$\frac{a^3}{D(t)^3} e^{-imf(t)} = \sum_{N=-\infty}^{\infty} F_{Nm} e^{-iN\Omega t}. \quad (7)$$

The F_{Nm} can be written explicitly as an integral over the eccentric anomaly ([Murray & Dermott 1999; Storch & Lai 2013](#)):

$$F_{Nm} = \frac{1}{\pi} \int_0^\pi \frac{\cos [N(E - e \sin E) - mf(E)]}{(1 - e \cos E)^2} dE. \quad (8)$$

By considering the effect of each summand in Eq. (5), the total torque on the star, energy transfer in the inertial frame, and energy transfer in the star’s corotating frame (which is also the tidal heating rate) can be obtained ([Storch & Lai 2013; Vick et al. 2017](#)):

$$T = \sum_{N=-\infty}^{\infty} F_{N2}^2 T_{\text{circ}}(N\Omega - 2\Omega_s), \quad (9)$$

$$\dot{E}_{\text{in}} = \frac{1}{2} \sum_{N=-\infty}^{\infty} \left\{ \left(\frac{W_{20}}{W_{22}} \right)^2 N\Omega F_{N0}^2 T_{\text{circ}}(N\Omega) + N\Omega F_{N2}^2 T_{\text{circ}}(N\Omega - 2\Omega_s) \right\}, \quad (10)$$

$$\dot{E}_{\text{rot}} = \dot{E}_{\text{in}} - \Omega_s T. \quad (11)$$

Here, dots indicate time derivatives.

Equations (9–10) can be used to express the binary orbital decay and circularization rates using

$$\frac{\dot{a}}{a} = -\frac{2a\dot{E}_{\text{in}}}{GMM_2}, \quad (12)$$

$$\frac{\dot{e}}{1 - e^2} = -\frac{a\dot{E}_{\text{in}}}{GMM_2} + \frac{T}{L_{\text{orb}}}, \quad (13)$$

where $L_{\text{orb}} = MM_2 [Ga(1 - e^2)/(M + M_2)]^{1/2}$ is the orbital angular momentum. The stellar spin synchronization rate can also be computed assuming that the star rotates rigidly:

$$\dot{\Omega}_s = \frac{T}{kMR^2}, \quad (14)$$

where kMR^2 is the moment of inertia of the MS star.

3 ANALYTIC EVALUATION OF TIDAL TORQUE AND ENERGY TRANSFER RATES

We can combine the expressions given in Sections 2.1 and 2.2 to compute the torque and energy transfer rate due to dynamical tides

in an eccentric binary. The tidal torque is obtained by evaluating Eq. (9) with the circular torque set to Eq. (1), giving:

$$T = \sum_{N=-\infty}^{N=\infty} F_{N2}^2 T_0 \operatorname{sgn} \left(N - \frac{2\Omega_s}{\Omega} \right) \left| N - \frac{2\Omega_s}{\Omega} \right|^{8/3}. \quad (15)$$

The energy transfer rate in the inertial frame is obtained by evaluating Eq. (10) in the same way, giving:

$$\dot{E}_{\text{in}} = \frac{T_0}{2} \sum_{N=-\infty}^{\infty} \left[N \Omega F_{N2}^2 \operatorname{sgn} \left(N - \frac{2\Omega_s}{\Omega} \right) \left| N - \frac{2\Omega_s}{\Omega} \right|^{8/3} + \left(\frac{W_{20}}{W_{22}} \right)^2 \Omega F_{N0}^2 |N|^{11/3} \right]. \quad (16)$$

These two expressions can be used to obtain the orbital decay, circularization, and spin synchronization rates using Eqs. (12–14).

While exact, the two sums in Eqs. (15–16) are difficult to evaluate for larger eccentricities, where one often must sum hundreds or thousands of terms, each of which has a different F_{Nm} . In the following, we obtain closed-form approximations to Eqs. (15–16) when the eccentricity is large.

3.1 Approximating Hansen Coefficients

To simplify Eqs. (15–16), we seek tractable approximations for both F_{N2} and F_{N0} . Note that while the Hansen coefficients can be evaluated using the integral expression Eq. (8), this requires calculating a separate integral for each N . Instead, it is more convenient to use the discrete Fourier Transform of the left hand side of Eq. (7) to calculate arbitrarily many N at once (as pointed out by Correia et al. 2014). Since $F_{(-N)m} = F_{N(-m)}$, we will only study the Hansen coefficient behavior for $m \geq 0$.

3.1.1 $m = 2$ Hansen Coefficients

Figure 1 shows F_{N2} vs. N when $e = 0.9$. First, we note that F_{N2} is much larger when $N \geq 0$ than for $N < 0$, so we focus on the behavior for $N \geq 0$. Here, F_{N2} has only one substantial peak. There are only two characteristic frequency scales: Ω and Ω_p , the pericentre frequency, defined by

$$\Omega_p \equiv \Omega \frac{\sqrt{1+e}}{(1-e)^{3/2}}. \quad (17)$$

For convenience, we also define N_p as the floor of Ω_p/Ω , i.e.

$$N_p \equiv \lfloor \Omega_p/\Omega \rfloor, \quad (18)$$

We find that the peak of the F_{N2} occurs at $N \sim N_p$, the only characteristic scale in N over which F_{N2} can vary. When $N \gg N_p$, the Fourier coefficients must fall off exponentially by the Paley-Wiener theorem, as the left hand side of Eq. (7) is smooth (e.g. Stein & Shakarchi 2009). When instead $N \ll N_p$, there are no characteristic frequencies between Ω and Ω_p , so we expect the Hansen coefficients to be scale-free between $N = 1$ and N_p , i.e. a power law in N . The expected behaviors in both of these regimes are in agreement with Fig. 1.

Motivated by these considerations, we approximate the Hansen coefficients by

$$F_{N2} \approx \begin{cases} C_2 N^p e^{-N/\eta_2} & N \geq 0, \\ 0 & N < 0, \end{cases} \quad (19)$$

for some fitting coefficients C_2 , p , and η_2 . By performing fits to F_{N2} ,

we find that $p \approx 2$ for substantial eccentricities, and we fix $p = 2$ for the remainder of this work¹.

To constrain the remaining two free parameters η_2 and C_2 , we use the well known Hansen coefficient moments

$$\sum_{N=-\infty}^{\infty} F_{N2}^2 = \frac{f_5}{(1-e^2)^{9/2}}, \quad (20)$$

$$f_5 \equiv 1 + 3e^2 + \frac{3e^4}{8}, \quad (21)$$

$$\sum_{N=-\infty}^{\infty} F_{N2}^2 N = \frac{2f_2}{(1-e^2)^6}, \quad (22)$$

$$f_2 \equiv 1 + \frac{15e^2}{2} + \frac{45e^4}{8} + \frac{5e^6}{16}. \quad (23)$$

Applying Eq. (19) to Eqs. (20, 22), we obtain the coefficients η_2 and C_2

$$\eta_2 = \frac{4f_2}{5f_5 (1-e^2)^{3/2}} \sim \frac{1}{2(1-e)^{3/2}}, \quad (24)$$

$$C_2 = \left[\frac{4f_5}{3(1-e^2)^{9/2} \eta_2^5} \right]^{1/2}. \quad (25)$$

Figure 1 illustrates the agreement of Eq. (19) using these two values of η_2 and C_2 with the numerical F_{N2} . The good agreement for $N \gtrsim N_p/10$ (which is where F_{N2} is large) is especially impressive as there are no fitting parameters in Eq. (19), as C_2 , η_2 , and p are all analytically constrained. Finally, note that the maximum of the F_{N2} occurs at $N = \lfloor 2\eta_2 \rfloor \sim (1-e)^{-3/2} \sim N_p$.

3.1.2 $m = 0$ Hansen Coefficients

We now turn to the $m = 0$ Hansen coefficients, F_{N0} , which are shown in Fig. 2. We know that $F_{N0} = F_{(-N)0}$, so we consider only $N \geq 0$. From the figure, we see that the F_{N0} decay exponentially. There is only one characteristic scale available for this decay, namely N_p . Therefore, we naturally assume the F_{N0} coefficients can be approximated by a function of form:

$$F_{N0} = C_0 e^{-|N|/\eta_0}. \quad (26)$$

¹ There is good reason to expect $p = 2$ for $N \ll N_p$ as long as the eccentricity is sufficiently large, as then the left-hand side of Eq. (7) resembles the second derivative of a Dirac delta function within each orbital period: It is both sharply peaked about $t = 0$ and has zero derivative three times every period (at $t = \epsilon$, $t = P/2$, and $t = P - \epsilon$ for some small $\epsilon \sim \Omega_p^{-1}$). These two characteristics describe the second derivative of a Gaussian with width $\sim \Omega_p^{-1}$. Then, for timescales longer than its width, a Gaussian resembles a Dirac delta function, which has a flat Fourier spectrum ($\propto N^0$). Finally, since time differentiation multiplies by N in frequency space, the second derivative of a Gaussian has a Fourier spectrum $\propto N^2$ for sufficiently small $N \lesssim N_p$. As F_{N2} is the N th Fourier coefficient for a function resembling the second derivative of a Dirac delta function for $N \lesssim N_p$, we do indeed expect $F_{N2} \propto N^2$ in this regime.

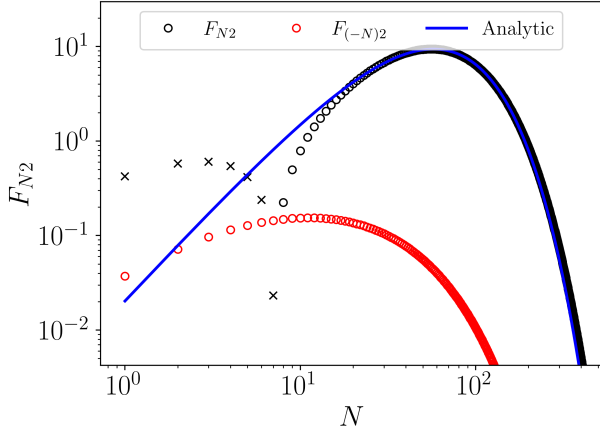


Figure 1. Plot of Hansen coefficients F_{N2} for $e = 0.9$. The red circles denote negative N , while the black circles and crosses denote positive and negative F_{N2} . The blue line is the formula given by Eq. (19) with η_2 and C_2 given by Eqs. (24–25).

The two free parameters C_0 and η_0 are constrained by the identities

$$\sum_{N=-\infty}^{\infty} F_{N0}^2 = \frac{f_5}{(1-e^2)^{9/2}}, \quad (27)$$

$$\sum_{N=-\infty}^{\infty} F_{N0}^2 N^2 = \frac{9e^2}{2(1-e^2)^{15/2}} f_3, \quad (28)$$

$$f_3 = \frac{1}{2} + \frac{15e^2}{8} + \frac{15e^4}{16} + \frac{5e^6}{128}. \quad (29)$$

Applying Eq. (26) to Eqs. (27–28), we obtain

$$\eta_0 = \left[\frac{9e^2 f_3}{(1-e^2)^3 f_5} \right]^{1/2}, \quad (30)$$

$$C_0 = \left[\frac{f_5}{(1-e^2)^{9/2} \eta_0} \right]^{1/2}. \quad (31)$$

Figure 2 illustrates the agreement of Eq. (26) using these two values of η_0 and C_0 with the numerically computed F_{N0} .

3.2 Approximate Expressions for Torque and Energy Transfer

Having found good approximations for the Hansen coefficients, we now apply them to simplify the expressions for the torque and the energy transfer rate in Eqs. (15–16).

3.2.1 Tidal Torque

To simplify Eq. (15), we replace F_{N2} with Eq. (19) and the sum with an integral, obtaining

$$T \approx T_0 \int_0^{\infty} C_2^2 N^4 e^{-2N/\eta_2} \operatorname{sgn}(N - 2\Omega_s/\Omega) |N - 2\Omega_s/\Omega|^{8/3} dN. \quad (32)$$

This expression is already easier to evaluate than Eq. (15), but we can use further approximations to obtain a closed form. We first

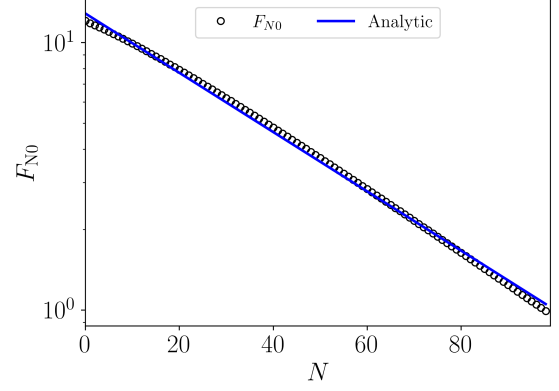


Figure 2. Plot of F_{N0} (black circles) for $e = 0.9$. Since $F_{N0} = F_{(-N)0}$, we only show positive N . The blue line is given by Eq. (26) with η_0 and C_0 given by Eqs. (30–31).

analyze Eq. (32) in the small-spin limit, where it can be integrated analytically², giving

$$T (|\Omega_s| \ll \Omega_p) \approx T_0 \frac{f_5(e) (\eta_2/2)^{8/3} \Gamma(23/3)}{(1-e^2)^{9/2} 4!}. \quad (33)$$

Note that this has the scaling $T \sim T_0 (1-e)^{-17/2} \sim T_p \Omega/\Omega_p$, where T_p is the torque exerted by a circular orbit with separation equal to the pericentre separation $a_p \equiv a(1-e)$, i.e.

$$T_p = \beta_2 \frac{GM_c^2 r_c^5}{a_p^6} \left(\frac{\Omega_p}{\sqrt{GM_c/r_c^3}} \right)^{8/3} \frac{\rho_c}{\bar{\rho}_c} \left(1 - \frac{\rho_c}{\bar{\rho}_c} \right)^2 \sim T_0 (1-e)^{-10}. \quad (34)$$

The top panel of Fig. 3 compares Eq. 33 to the integral of Eq. (32) and to the direct sum of Eq. (15) as a function of the eccentricity. It can be seen that both the integral and the analytic closed form perform well for moderate-to-large eccentricities, but both over-predict the torque at small $e \lesssim 0.3$. This discrepancy is expected: there are only a few non-negligible summands in Eq. (15) when e is small, so replacing the sum over N with an integral is expected to introduce significant inaccuracy that appears in both the integral and closed-form expressions.

Eq. (33) is valid so long as $|\Omega_s/\Omega| \ll N_{\max}$ (or equivalently, $|\Omega_s \ll \Omega_p|$), where $N_{\max} = 10\eta_2/3$ is where the integrand is in Eq. (32) maximized. If instead $|\Omega_s/\Omega| \gg N_{\max}$, the torque can be evaluated directly using Eq. (15) and the known Hansen coefficient moments, giving:

$$T (|\Omega_s| \gg \Omega_p) \approx -T_0 \operatorname{sgn}(\Omega_s) |2\Omega_s/\Omega|^{8/3} \frac{f_5(e)}{(1-e^2)^{9/2}}. \quad (35)$$

The bottom panel of Fig. 3 compares this formula to the integral of Eq. (32) and to the direct sum of Eq. (15) as a function of the eccentricity, where $\Omega_s/\Omega = 400$. Here, $N_{\max} \ll 400$ for all eccentricities shown. We see that direct summation, the integral expression, and Eq. (35) agree very well for all eccentricities.

Having obtained closed-form expressions of Eq. (32) for small

² The key to the success of our approach is that sums of form $\sum_{n=-\infty}^{\infty} F_{N2}^2 N^p$ can be approximated for non-integer p in terms of the Γ function, since $\int_0^{\infty} x^p e^{-x} dx = \Gamma(p+1)$.

and large spins, we can further derive a single expression joining these two limits. To do this, we first assume that the spin is small but non-negligible. In this regime, we make the approximation

$$N - 2\Omega_s/\Omega \approx \frac{N}{N_{\max}} \left(N_{\max} - \frac{2\gamma_T \Omega_s}{\Omega} \right), \quad (36)$$

for some free parameter γ_T . With this, we can integrate Eq. (32) in closed form. We can fix γ_T by requiring our expression reproduce the large spin limit (Eq. 35) when taking $|\Omega_s| \rightarrow \infty$. This procedure gives an expression for the torque that agrees with both limiting forms (Eq. 33–35) and is given by

$$T \approx T_0 \frac{f_5(e)(\eta_2/2)^{8/3}}{(1-e^2)^{9/2}} \operatorname{sgn} \left(1 - \gamma_T \frac{\Omega_s}{\eta_2 \Omega} \right) \left| \frac{4}{\gamma_T} \left(1 - \gamma_T \frac{\Omega_s}{\eta_2 \Omega} \right) \right|^{8/3}, \quad (37)$$

where

$$\gamma_T = 4 \left(\frac{4!}{\Gamma(23/3)} \right)^{3/8} \approx 0.691. \quad (38)$$

Figure 4 compares this expression to the integral of Eq. (32) and to the direct sum of Eq. (15) at fixed $e = 0.9$ and varying Ω_s . We see that Eq. (37) agrees well with the integral and sum for both large and small spins, and is also reasonably accurate for intermediate spins. However, Eq. (32) is more accurate than Eq. (37) when T changes signs and $|T|$ is small. This is also expected: T changes signs when the spin approaches (Section 3.2.2) because large contributions to the sum in Eq. (15) have opposite signs and mostly cancel out. Thus, small inaccuracies in the summand result in significant discrepancies in the total torque. The integral approximation, Eq. (32), is expected to be in good agreement with the direct sum, Eq. (15), as the accuracy of the Hansen coefficient approximation in Section 3.1 is good for large eccentricities, thus guaranteeing term-by-term accuracy. On the other hand, the closed-form expression, Eq. (37), is more approximate when $\Omega_s/\Omega \sim N_{\max} \sim \eta_2$. In fact, Eq. (37) predicts $dT/d\Omega_s \approx 0$ near $\Omega_s = 0$. This is not accurate and is an artifact of our factorization ansatz in Eq. (36).

In summary, the tidal torque must be evaluated with explicit summation (Eq. 15) when $e \lesssim 0.3$ (see discussion after Eq. 33), can be approximated by the integral expression (Eq. 32) when e is large for all values of Ω_s , and otherwise can be approximated by the closed-form expression given by Eq. (37). Recall that when e is small, the explicit summation of Eq. (15) is quite simple, as good accuracy can be obtained with just the first few terms in the summation.

3.2.2 Pseudosynchronization

In general, the exact torque as given by Eq. (15) vanishes for a single Ω_s , which we call the *pseudo-synchronized* spin frequency. An approximation for the pseudo-synchronized spin can be directly read off from Eq. (37):

$$\frac{\Omega_{\text{ps}}}{\Omega} = \frac{\eta_2}{\gamma_T} = \frac{4f_2(e)}{5\gamma_T f_5(e) (1-e^2)^{3/2}}. \quad (39)$$

This has the expected scaling $\Omega_{\text{ps}} \sim \Omega_p$ (the pericentre orbital frequency). Figure 5 compares this prediction for the pseudo-synchronized spin to the exact one obtained by applying a root finding algorithm to Eq. (15). We see that Eq. (39) is a good approximation for the pseudo-synchronized spin frequency when $e \gtrsim 0.1$.

In passing, we note that, in the standard weak friction theory of

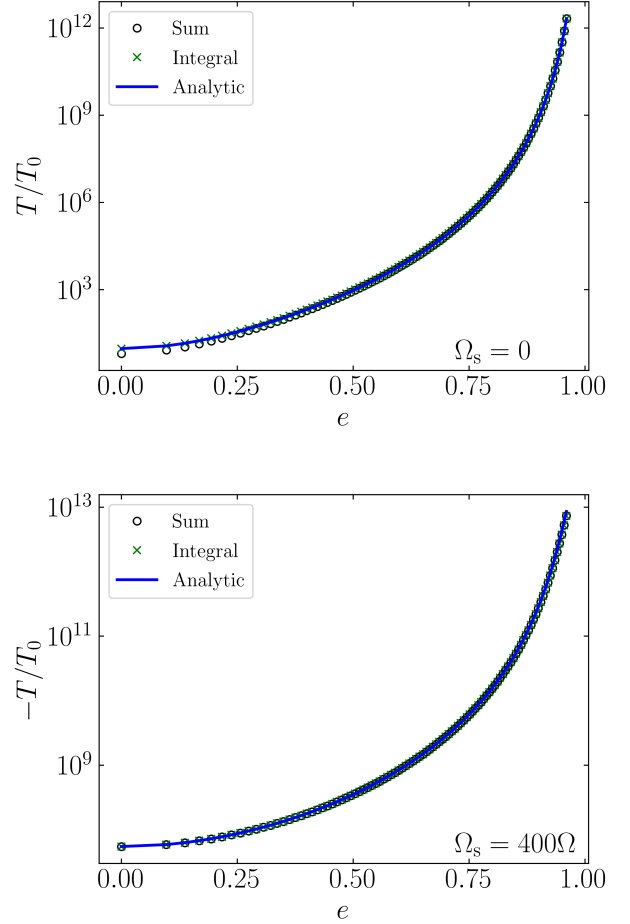


Figure 3. The tidal torque on a non-rotating (top) and rapidly rotating (bottom) star due to a companion with orbital eccentricity e . Black circles represent direct summation of Eq. (15), green crosses are evaluated using the integral approximation Eq. (32), and the blue line is Eq. (37). In the small and large spin limits, Eq. (37) reduces to Eq. (33) and Eq. (35) respectively.

equilibrium tides, the pseudo-synchronized spin is given by (Alexander 1973; Hut 1981)

$$\frac{\Omega_{\text{ps}}^{(\text{Eq})}}{\Omega} = \frac{f_2(e)}{f_5(e) (1-e^2)^{3/2}}. \quad (40)$$

Though describing a different tidal phenomenon, this only differs from Eq. (39) by a factor of $4/(5\gamma_T) \approx 1.15$. We show it for comparison as the red dotted line in Fig. 5.

3.2.3 Energy Transfer

We now turn our attention to Eq. (10) and replace F_{N2} and F_{N0} with their respective approximations (Eqs. 19 and 26) to obtain the energy transfer rate

$$\begin{aligned} \dot{E}_{\text{in}} = & \frac{T_0 \Omega}{2} \int_0^\infty \left[C_2^2 N^5 e^{-2N} / \eta_2 \operatorname{sgn}(N - 2\Omega_s/\Omega) |N - 2\Omega_s/\Omega|^{8/3} \right. \\ & \left. + 2 \left(\frac{W_{20}}{W_{22}} \right)^2 C_0^2 e^{-2N} / \eta_0 N^{11/3} \right] dN. \end{aligned} \quad (41)$$

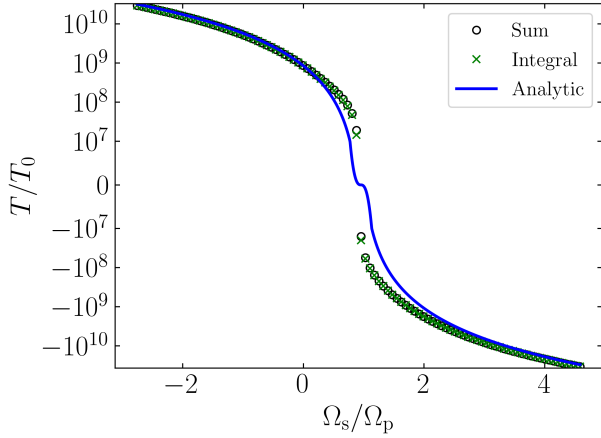


Figure 4. The tidal torque as a function of the stellar spin for a highly eccentric $e = 0.9$ companion. The black circles represent direct summation of Eq. (15), green crosses the integral approximation (Eq. 32), and the solid line the analytic closed-form expression Eq. (37). The spin is normalized by the pericentre orbital frequency $\Omega_p \approx 43\Omega$ (Eq. 17).

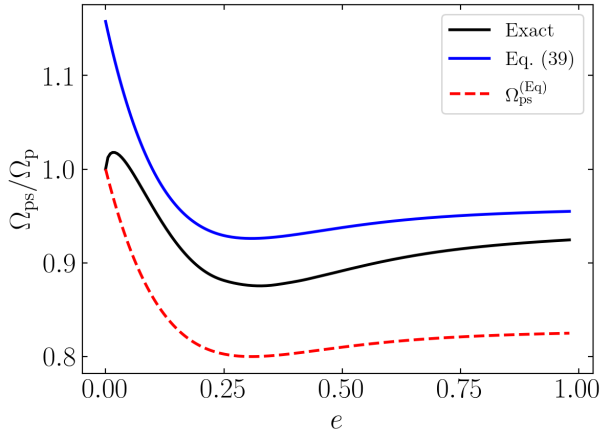


Figure 5. The spin frequencies Ω_{ps} normalized by the pericentre frequency Ω_p (Eq. 17) as a function of eccentricity. The blue line is given by Eq. (39). The black line shows the exact solution, obtained by using a root finding algorithm to solve for the zero of Eq. (9). The red dashed line shows the spin frequency predicted by the weak friction theory of equilibrium tides (Eq. 40).

We evaluate the $m = 2$ and $m = 0$ contributions to this expression separately.

We first examine the $m = 2$ contribution using the same procedure in Section 3.2.1 for the torque. If the spin is moderate, i.e. $|\Omega_s/\Omega| \lesssim N_{\max}$ where now $N_{\max} = 23\eta_2/6$, we make the approximation

$$N - 2\Omega_s/\Omega \approx \frac{N}{N_{\max}} \left(N_{\max} - \frac{2\gamma_E \Omega_s}{\Omega} \right), \quad (42)$$

where γ_E is a free parameter. This lets us integrate the $m = 2$ contribution to Eq. (41) analytically. We constrain γ_E by requiring agreement with the large-spin limit: for $|\Omega_s/\Omega| \gg N_{\max}$, we have

$$\dot{E}_{\text{in}}^{(m=2)} (|\Omega_s| \gg \Omega_p) \approx -\frac{T_0 \Omega}{2} \text{sgn}(\Omega_s) |2\Omega_s/\Omega|^{8/3} \frac{2f_2(e)}{(1-e^2)^6}. \quad (43)$$

This fixes γ_E and we obtain the complete $m = 2$ contribution to Eq. (41):

$$\begin{aligned} \dot{E}_{\text{in}}^{(m=2)} &\approx \frac{T_0 \Omega f_5(e) (\eta_2/2)^{11/3}}{2(1-e^2)^{9/2}} \\ &\times \text{sgn} \left(1 - \gamma_E \frac{\Omega_s}{\eta_2 \Omega} \right) \left| \frac{4}{\gamma_E} \left(1 - \gamma_E \frac{\Omega_s}{\eta_2 \Omega} \right) \right|^{8/3}, \end{aligned} \quad (44)$$

where

$$\gamma_E = 4 \left(\frac{5!}{\Gamma(26/3)} \right)^{3/8} \approx 0.5886. \quad (45)$$

Note that, when $\Omega_s \approx 0$, Eq. (44) gives the expected scaling of $\dot{E}_{\text{in}}^{(m=2)} \sim T_p \Omega$ where T_p is the torque exerted by a circular companion at the pericentre separation, given by Eq. (34).

The $m = 0$ contribution to Eq. (41) can be straightforwardly integrated using the parameterization Eq. (26). The sum of the two contributions then gives the total energy transfer rate:

$$\begin{aligned} \dot{E}_{\text{in}} &= \frac{T_0 \Omega}{2} \left[\frac{f_5(e) (\eta_2/2)^{11/3}}{(1-e^2)^{9/2}} \right. \\ &\times \text{sgn} \left(1 - \gamma_E \frac{\Omega_s}{\eta_2 \Omega} \right) \left| \frac{4}{\gamma_E} \left(1 - \gamma_E \frac{\Omega_s}{\eta_2 \Omega} \right) \right|^{8/3} \\ &\left. + \frac{f_5(e) \Gamma(14/3)}{(1-e^2)^{10}} \left(\frac{3}{2} \right)^{8/3} \left(\frac{e^2 f_3(e)}{f_5(e)} \right)^{11/6} \right]. \end{aligned} \quad (46)$$

The two panels of Fig. 6 compare this expression with the integral form Eq. (41) and the direct sum Eq. (16) for small and large spins. The agreements are excellent except that, when the spin and eccentricity are small, both the integral and closed form expressions over-predict the energy transfer rate. Figure 7 compares these three expressions as a function of spin for $e = 0.9$. The performance of Eq. (46) degrades when the system is near ($\Omega_s \approx \Omega_p$), but generally captures the correct behavior of the exact result, while Eq. (41) is accurate for all spins. As was the case with the tidal torque, we see that the evaluation of the energy transfer rate when $e \lesssim 0.3$ requires direct summation (Eq. 16), and the evaluation when e is substantial but the spin is near can be performed using the integral approximation (Eq. 41), and otherwise the evaluation can be performed using the closed-form expression (Eq. 46).

4 PSR J0045-7319/B-STAR BINARY

As an application of our analytical results above, we consider the PSR J0045-7319/MS binary system (Kaspi et al. 1994) and attempt to explain its orbital decay via dynamical tides. This system is one of the few pulsar binaries discovered so far that have massive MS companions (the other known binaries are, PSR B1259-63, PSR J1740-3052, PSR J1638-4725, J2032+4127; Johnston et al. 1992; Stairs et al. 2001; Lorimer et al. 2006; Lyne et al. 2015). These systems evolve from MS-MS binaries when one of the stars explodes in a supernova to form a neutron star (NS), and will eventually become double NS systems when the MS companion also explodes to form a NS. Thus, characterizing the evolution of such systems is important for understanding the formation of double NS binaries (e.g. Tauris et al. 2017). The PSR J0045-7319 system contains a radio pulsar ($M_2 \approx 1.4M_\odot$) and a massive B star ($M \approx 8.8M_\odot$) companion in an eccentric ($e = 0.808$) orbit with period $P = 51.17$ days, corresponding to a semi-major axis $a = 126R_\odot$. Timing observation shows that the orbit is decaying at the rate $\dot{P} = -3.03 \times 10^{-7}$, or $P/\dot{P} \approx -0.5$ Myr (Kaspi et al. 1996). The measured B-star luminosity

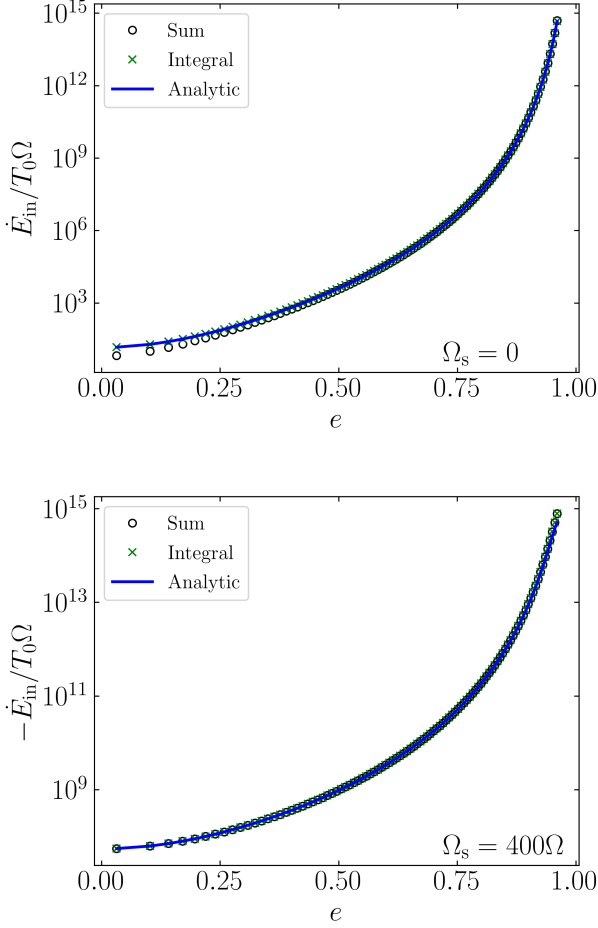


Figure 6. The tidal energy transfer rate \dot{E}_{in} for a non-rotating (top) and a rapidly rotating (bottom) star. The black circles represent direct summation of Eq. (16), green crosses the integral form Eq. (41), and the blue line the closed-form expression Eq. (46).

$L = 1.2 \times 10^4 L_{\odot}$ and surface temperature $T_{\text{surf}} = (24000 \pm 1000)$ K imply a radius of $R = 6.4 R_{\odot}$ (Bell et al. 1995). The B star has a projected surface rotation velocity $v \sin i = 113 \pm 10$ km/s (Bell et al. 1995), consistent with rapid rotation (the breakup velocity is $\sqrt{GM/R} = 512$ km/s). While there are uncertainties in some of these parameters (e.g., the pulsar and companion masses could be larger by about 10%; see Thorsett & Chakrabarty 1999), we adopt the above values in our calculation below for better comparison with previous works.

Lai (1996) and Lai (1997) explained the observed orbital decay of the PSR J0045 binary in terms of tidal excitations of discrete (rotation-modified) g-modes followed by radiative damping. He showed that retrograde rotation of the B-star (consistent with the observed nodal precession of the binary orbit; see Lai et al. 1995; Kaspi et al. 1996) can significantly enhance the strength of mode excitation, and potentially account for the observed orbital decay, although he did not compute the mode damping rate quantitatively. Kumar & Quataert (1997, 1998) examined the damping of g-modes and showed that radiative damping in rigidly rotating B-star is inadequate to explain the observed orbital decay rate, suggesting that in addition to retrograde rotation, significant differential rotation or

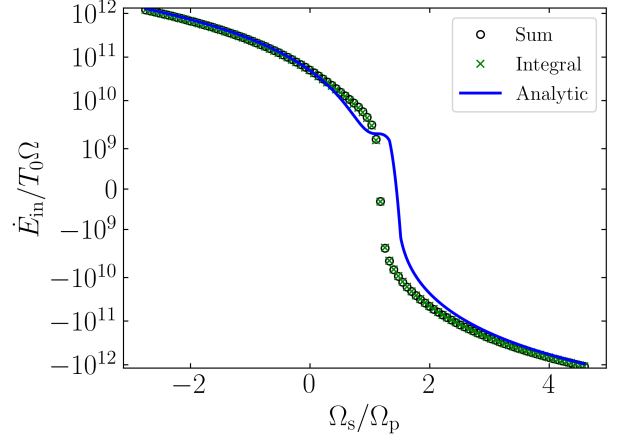


Figure 7. The tidal energy transfer rate \dot{E}_{in} as a function of spin [normalized by Ω_p ; Eq. (17)] for a highly eccentric $e = 0.9$ companion. The black circles represent direct summation of Eq. (10), green crosses the integral approximation Eq. (41), and the blue line the analytic closed form Eq. (46).

nonlinear parametric mode decay may be required. Given the uncertainties in their estimates, it was not clear to what extent the observed orbital decay rate can be quantitatively explained. Moreover, both Lai et al. (1995) and Kumar & Quataert (1997, 1998) considered discrete g-modes, whereas absorption of tidally excited gravity waves near the stellar envelope, via either efficient radiative damping or nonlinear breaking (see Su et al. 2020), implies outgoing waves (as adopted in the works of Zahn 1975; Goldreich & Nicholson 1989; Kushnir et al. 2017) rather than discrete g-modes.

We now consider the evolution of stellar spin and binary orbit for the PSR J0045-7319 system. For the adopted system parameters above, the pericentre distance is $a_p \approx 3.78R$, and pericentre frequency is $\Omega_p = \sqrt{(1+e)GM_{\text{tot}}/a_p^3} \approx 0.20\sqrt{GM/R^3}$. First we note that the tidal torque T and the energy transfer rate \dot{E}_{in} (dominated by the $m = 2$ term) are related by

$$\dot{E}_{\text{in}} \approx T \Omega_p \frac{f_2}{5(1+e)^2 f_5}, \quad (47)$$

with $f_2 = 8.38$, $f_5 = 3.12$. Thus the spin evolution rate (for spin-orbit synchronization and alignment) is given by

$$\left| \frac{\dot{S}}{S} \right| \approx \frac{L}{S} \frac{5(1-e^2)f_5}{2f_2} \left| \frac{\dot{E}_{\text{in}}}{E_{\text{orb}}} \right|, \quad (48)$$

where $S = kMR^2\bar{\Omega}_s$ is the spin angular momentum of the star (with $\bar{\Omega}_s$ the mean rotation rate, and $k \approx 0.1$), L is the orbital angular momentum, and E_{orb} is the orbital energy. Thus

$$\left| \frac{\dot{S}}{S} \right| \approx 6.3 \frac{\Omega_p}{\bar{\Omega}_s} \left| \frac{\dot{a}}{a} \right|. \quad (49)$$

The observed nodal precession of the PSR J0045-7319 binary implies that the spin of the B-star is far from spin-orbit alignment and synchronization driven by tides (Lai et al. 1995). Thus we require $\bar{\Omega}_s \gtrsim 6.3\Omega_p \sim \sqrt{GM/R^3}$, suggesting that the internal rotation rate of the star is much larger than the surface rate.

Using Eq. (46) with $e = 0.808$ (and keeping only the $m = 2$ term),

we find that the orbital decay rate is given by

$$\left| \frac{\dot{a}}{a} \right| \approx 1.6 \times 10^5 \Omega \frac{M_2}{M} \left(\frac{M_{\text{tot}}}{M_c} \right)^{4/3} \times \left(\frac{r_c}{a} \right)^9 \frac{\rho_c}{\bar{\rho}_c} \left(1 - \frac{\rho_c}{\bar{\rho}_c} \right)^2 \left| \frac{4}{\gamma_E} \left(1 - \frac{\gamma_E \Omega_s}{\eta_2 \Omega} \right) \right|^{8/3}. \quad (50)$$

With $\eta_2 = 10.55$, $a \approx 19.7R$, and adopting $\rho_c/\bar{\rho}_c \approx 1/3$, we find the orbital decay rate

$$\left| \frac{\dot{P}}{P} \right| \approx \frac{1}{0.5 \text{ Myr}} \left(\frac{3M_\odot}{M_c} \right)^{4/3} \left(\frac{r_c}{0.54R} \right)^9 \left| 1 - \frac{0.89\Omega_s}{\Omega_p} \right|^{8/3}. \quad (51)$$

Note Ω_s in the above expression refers to the rotation rate at the radiative-convective boundary (RCB) r_c , and we expect $\Omega_s \gtrsim \bar{\Omega}_s \gtrsim 6\Omega_p$.

To explain the observed orbital decay timescale $|P/\dot{P}| \approx 0.5$ Myr, the most critical parameter is the core radius r_c . Kumar & Quataert (1998) adopted $M_c \approx 3M_\odot$ and $r_c \approx 1.38R_\odot$ (or $r_c \approx 0.22R$) based on comparison with a Yale stellar evolution model. This value of r_c would require $\Omega_s/\Omega_p \approx -24$, or $\Omega_s \approx -4.8\sqrt{GM/R^3}$, to explain the observed decay rate. If we use a slightly larger core radius, $r_c = 1.5R_\odot \approx 0.234R$, the required Ω_s would be $\Omega_s \approx -18\Omega_p \approx -3.6\sqrt{GM/R^3}$. In either case, extreme differential rotation (with $|\Omega_s|$ at the RCB at least a factor of few larger than the surface rotation) is required. In Fig. 8 we show \dot{P}/P as a function of Ω_s , obtained using the exact expression Eq. (46) for four different values of r_c . In general, given that the surface rotation rate of the star is less than $\sqrt{GM/R^3}$, our calculation suggests that the B-star must have large, retrograde differential rotation in order to explain the observed orbital decay.

We note that our own exploration of stellar models using the Modules for Experiments in Stellar Astrophysics (MESA; Paxton et al. 2011, 2013, 2015, 2018, 2019) generally finds a small core radius ($r_c \lesssim R_\odot$) for the B-star in the PSR J0045-7319 system. Since the system is in the Small Magellanic Cloud, we use a typical metallicity $Z = 0.1Z_\odot$, where Z_\odot is the solar metallicity. For a range of initial stellar masses, we begin with a non-rotating zero-age main sequence (ZAMS) stellar model, and evolve it until its core hydrogen is depleted. Among these evolutionary tracks, we select the model and stellar age that best matches the observed L and T_{surf} and record the core radius at that age. We then repeat this procedure with different values for the convective overshoot parameter, initial rotation rate (up to nearly maximally rotating), and metallicity (up to $Z = 0.2Z_\odot$). For all parameter combinations, the predicted stellar masses lie in the range $8.8M_\odot \leq M \leq 10M_\odot$, in agreement with the estimates in the literature. However, the core radius for all stellar models is $r_c \lesssim R_\odot \approx 0.16R$. This reflects the fact that our best-fitting stellar models tend to be somewhat evolved from the ZAMS.

We caution that applying standard isolated stellar evolution to the B-star in the PSR J0045-7319 system can be fraught with uncertainties. The very rapid rotation may induce instabilities and allow the star to transport material from the hydrogen-rich envelope into the central burning region and vice versa, potentially making the convective core larger (e.g. Maeder 1987; Heger & Langer 2000). This effect may be enhanced by the large misaligned, differential rotation. Related to the rotational effect is the mass transfer effect: The observed rapid orbital decay rate and general orbital evolution modeling sets an upper limit of about 1.4 Myr on the age of the binary system since the last supernova explosion (Lai 1996), much shorter than the canonical MS lifetime. Thus the B-star must have accreted significant material from the pulsar progenitor in the recent past. Such accretion can affect the structure and evolution of the B-star in a significant way. Given these uncertainties, we think it is likely that the B-star

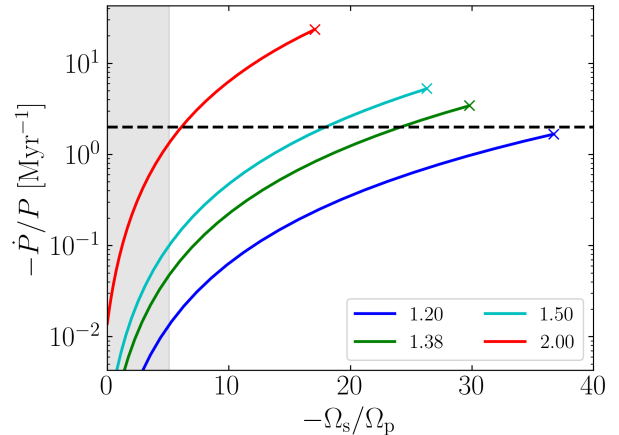


Figure 8. The orbital decay ratio \dot{P}/P as a function of Ω_s for the canonical parameters of the PSR J0045-7319 binary system, as evaluated by Eq. (46), for four different values of r_c (legend, in units of R_\odot). The measured $\dot{P}/P = -(0.5 \text{ Myr})^{-1}$ is shown by the horizontal dashed line. The vertical shaded region is the region where $|\Omega_s|$ is less than the breakup rotation rate of the star as a whole, given by $(GM/R^3)^{1/2}$. Each r_c is only shown for $|\Omega_s| \leq \Omega_{s,c} \equiv (GM_c/r_c^3)^{1/2}$, the core breakup rotation rate, and the colored crosses denote where $\Omega_s = \Omega_{s,c}$ for each value of r_c . Note that for $r_c \lesssim 1.3R_\odot$, even a maximally rotating core cannot generate enough tidal torque to match the observed \dot{P}/P .

has a larger core radius than the canonical value, rendering a less extreme differential rotation³.

5 SUMMARY AND DISCUSSION

5.1 Key Results

The main goal of this paper is to derive easy-to-use, analytical expressions for the tidal torque T and tidal energy transfer rate \dot{E}_{in} due to internal gravity wave (IGW) dissipation in a massive, main-sequence (MS) star under the gravitational influence of an eccentric companion. Tidal evolution in such systems plays an important role in the formation scenarios of merging neutron-star (NS) binaries. For general eccentricities, these expressions are given by the sums, Eqs. (15) and (16), respectively. However, when the eccentricity is large, these sums require the evaluation of many terms to be accurate. We have derived approximate expressions in two regimes:

- For $e \gtrsim 0.3$, we show that the tidal torque and energy transfer rate can be accurately approximated by the integral expressions, Eqs. (32) and (41).
- If furthermore the spin of the stellar core is not very close to its pseudo-synchronized value (i.e. where the torque vanishes; see Section 3.2.2), we show that these two integral expressions can be well approximated by the closed-form expressions, Eqs. (37) and (46).

These analytical expressions for T and \dot{E}_{in} (particularly the closed-form expressions) can be easily applied to study the spin and orbital evolution of eccentric binaries consisting of massive MS stars, such

³ We note that a recent study of intermediate and high-mass eclipsing binaries suggests that convective core masses are underpredicted by stellar structure codes (Tkachenko et al. 2020).

as those found in the evolution scenarios leading to the formation of merging neutron star binaries.

We then apply our analytical expressions to the PSR J0045-7319 binary system, which has a massive B-star companion and a measured orbital decay rate. This system provides a rare example to test/calibrate our theoretical understanding of IGW-mediated dynamical tides in massive stars. We show that for the “standard” radius of the convective core based on isolated non-rotating stellar modeling, the B-star must have a significant retrograde and differential rotation (with the rotation rate at the convective-radiative boundary at least a few times larger than the surface rotation rate of the star). Alternatively, we suggest that the convective core radius may be larger than the standard value as a result of rapid stellar rotation and/or mass transfer to the B-star in the recent past during the post-MS evolution of the pulsar progenitor. Overall, our attempt to explain the rapid orbital decay of the PSR J0045-7319 binary highlights the critical importance of internal stellar structure, particularly the size of the convective core, in determining the tidal evolution of eccentric binaries containing massive MS stars.

5.2 Caveats

Concerning our analytical expressions for the tidal torque and energy transfer rate, we note a few potential caveats:

(i) For simplicity, we have assumed that the stellar spin and orbit axes are aligned or anti-aligned. For general stellar obliquities (as in the case of the PSR J0045-7319 binary system), it is possible to decompose the tidal force into different Fourier components (see Appendix A of [Lai 1997](#)), and this would unlikely to yield qualitatively different result in terms of the orbital decay rate (cf. [Lai 2012](#)).

(ii) More importantly, in our work we have assumed that all Fourier harmonics (with different forcing frequencies $N\Omega$ in the inertial frame, where Ω is the mean orbital frequency) of the tidal potential excite IGWs at the radiative-convective boundary that damp completely as they propagate towards the stellar surface. This is known to be the case when the normalized tidal forcing frequency ω (equal to $N\Omega - 2\Omega_s$ for $m = 2$ and $N\Omega$ for $m = 0$) satisfies $|\omega| \ll \sqrt{GM/R^3}$ due to efficient radiative damping ([Zahn 1975](#); [Kushnir et al. 2017](#); see also the review paper [Ogilvie 2014](#)). Note that the dominant Fourier harmonics of the tidal potential have $N\Omega \sim \Omega_p$ (the orbital frequency at the pericentre). Thus, as long as $\Omega_p, |\Omega_s| \ll \sqrt{GM/R^3}$, the assumption of outgoing IGWs inherent in our theory is valid. When $|\omega|$ is comparable to $\sqrt{GM/R^3}$, it is traditionally thought that IGWs set up standing modes in the stellar interior. This is because IGWs are evanescent sufficiently near stellar surface, where the pressure scale height becomes smaller than the radial wavelength of the wave ([Goldreich & Nicholson 1989](#)). Moreover, [Su et al. \(2020\)](#) found that sufficiently large-amplitude IGWs can spontaneously cause a critical layer to form due to nonlinear wave breaking, causing incident IGWs to be efficiently absorbed. After such a critical layer forms, it can propagate to deep within the stellar interior and efficiently absorb IGWs even before they reach breaking amplitudes. Wave breaking and other nonlinear effects (such as nonlinear mode couplings) may be enhanced in an eccentric binary such as PSR J0045-7319, where IGWs with a wide range of frequencies are excited. [Burkart et al. \(2012\)](#) found that the frequency cutoff for g-modes in the eccentric heartbeat star system KOI-54 (with eccentricity $e = 0.83$, orbital period $P = 41.8$ days, and stellar mass $M \approx 2.3M_\odot$) is in agreement with the frequency at which IGWs become efficiently damped by thermal diffusion. However, in higher-mass MS stars such as that in PSR J0045-7319, nonlinear wave breaking may be an important

source of IGW damping due to the larger tidal torque. More work is needed to address whether our assumption of traveling IGWs in massive stars is accurate.

6 ACKNOWLEDGEMENTS

We thank Matteo Cantiello, Christopher O’Connor, Eliot Quataert, and Michelle Vick for fruitful discussions. YS is supported by the NASA FINESST grant 19-ASTRO19-0041. This work has been supported in part by NSF grants AST-1715246 and AST-2107796.

7 DATA AVAILABILITY

The data underlying this article will be shared on reasonable request to the corresponding author.

REFERENCES

- Alexander M., 1973, *Astrophysics and Space Science*, 23, 459
 Bell J., Bessell M., Stappers B., Bailes M., Kaspi V., 1995, *The Astrophysical Journal Letters*, 447, L117
 Burkart J., Quataert E., Arras P., Weinberg N. N., 2012, *Monthly Notices of the Royal Astronomical Society*, 421, 983
 Champion D. J., et al., 2008, *Science*, 320, 1309
 Correia A. C., Boué G., Laskar J., Rodríguez A., 2014, *Astronomy & Astrophysics*, 571, A50
 Goldreich P., Nicholson P. D., 1989, *Astrophysical Journal*, 342, 1079
 Heger A., Langer N., 2000, [ApJ](#), 544, 1016
 Hurley J. R., Tout C. A., Pols O. R., 2002, *Monthly Notices of the Royal Astronomical Society*, 329, 897
 Hut P., 1981, *Astronomy and Astrophysics*, 99, 126
 Janka H., Wongwathanarat A., Kramer M., et al., 2021, arXiv preprint arXiv:2104.07493
 Johnston S., Manchester R. N., Lyne A. G., Bailes M., Kaspi V. M., Qiao G., D’Amico N., 1992, [ApJ](#), 387, L37
 Johnston S., Manchester R., Lyne A., Nicastro L., Spyromilio J., 1994, *Monthly Notices of the Royal Astronomical Society*, 268, 430
 Kaspi V., Johnston S., Bell J., Manchester R., Bailes M., Bessell M., Lyne A. a., D’Amico N., 1994, *The Astrophysical Journal*, 423, L43
 Kaspi V., Bailes M., Manchester R., Stappers B., Bell J., 1996, *Nature*, 381, 584
 Kumar P., Quataert E. J., 1997, *The Astrophysical Journal Letters*, 479, L51
 Kumar P., Quataert E. J., 1998, *The Astrophysical Journal*, 493, 412
 Kushnir D., Zaldarriaga M., Kollmeier J. A., Waldman R., 2017, *Monthly Notices of the Royal Astronomical Society*, 467, 2146
 Lai D., 1996, *The Astrophysical Journal Letters*, 466, L35
 Lai D., 1997, [ApJ](#), 490, 847
 Lai D., 2012, *Monthly Notices of the Royal Astronomical Society*, 423, 486
 Lai D., Bildsten L., Kaspi V. M., 1995, [ApJ](#), 452, 819
 Lai D., Chernoff D. F., Cordes J. M., 2001, *The Astrophysical Journal*, 549, 1111
 Lorimer D. R., et al., 2006, [MNRAS](#), 372, 777
 Lyne A. G., Stappers B. W., Keith M. J., Ray P. S., Kerr M., Camilo F., Johnson T. J., 2015, [MNRAS](#), 451, 581
 Maeder A., 1987, *A&A*, 178, 159
 Murray C. D., Dermott S. F., 1999, *Solar system dynamics*. Cambridge university press
 Ogilvie G. I., 2014, *Annual Review of Astronomy and Astrophysics*, 52, 171
 O’Leary R. M., Burkart J., 2014, [Monthly Notices of the Royal Astronomical Society](#), 440, 3036
 Paxton B., Bildsten L., Dotter A., Herwig F., Lesaffre P., Timmes F., 2011, [ApJS](#), 192, 3
 Paxton B., et al., 2013, [ApJS](#), 208, 4
 Paxton B., et al., 2015, [ApJS](#), 220, 15

- Paxton B., et al., 2018, [ApJS](#), **234**, 34
- Paxton B., et al., 2019, [ApJS](#), **243**, 10
- Savonije G., Papaloizou J., 1983, *Monthly Notices of the Royal Astronomical Society*, **203**, 581
- Stairs I. H., et al., 2001, [MNRAS](#), **325**, 979
- Stein E. M., Shakarchi R., 2009, *Real analysis: measure theory, integration, and Hilbert spaces*. Princeton University Press
- Storch N. I., Lai D., 2013, *Monthly Notices of the Royal Astronomical Society*, **438**, 1526
- Su Y., Lecoanet D., Lai D., 2020, [Monthly Notices of the Royal Astronomical Society](#), **495**, 1239
- Tauris T. M., et al., 2017, [ApJ](#), **846**, 170
- Thorsett S. E., Chakrabarty D., 1999, *The Astrophysical Journal*, **512**, 288
- Tkachenko A., et al., 2020, *Astronomy & Astrophysics*, **637**, A60
- Vick M., Lai D., Fuller J., 2017, *Monthly Notices of the Royal Astronomical Society*, **468**, 2296
- Vick M., MacLeod M., Lai D., Loeb A., 2021, [MNRAS](#), **503**, 5569
- Vigna-Gómez A., MacLeod M., Neijssel C. J., Broekgaarden F. S., Justham S., Howitt G., de Mink S. E., Mandel I., 2020, arXiv preprint [arXiv:2001.09829](#)
- Yu H., Weinberg N. N., Fuller J., 2020, *Monthly Notices of the Royal Astronomical Society*, **496**, 5482
- Yu H., Fuller J., Burdge K. B., 2021, *Monthly Notices of the Royal Astronomical Society*, **501**, 1836
- Zahn J.-P., 1975, *Astronomy and Astrophysics*, **41**, 329
- Zaldarriaga M., Kushnir D., Kollmeier J. A., 2018, *Monthly Notices of the Royal Astronomical Society*, **473**, 4174

This paper has been typeset from a $\text{\TeX}/\text{\LaTeX}$ file prepared by the author.